Ceramic composite with the incorporation of graphene oxide self-assembly coated Si_3N_4 powders

Wenliang Zhang[1,a], Guangchun Xiao[1,b], Jingjie Zhang[1,c], Zhaoqiang Chen[1,d], Mingdong Yi[1,e] and Chonghai Xu[1,2,f*]

[1]School of Mechanical and Automotive Engineering, Qilu University of Technology (Shandong Academy of Sciences), Jinan 250353, China;

[2]Key Laboratory of Equipments Manufacturing and Intelligent Measurement and Control, China National Light Industry, Qilu University of Technology (Shandong Academy of Sciences), Jinan 250353, China

[a]zwliang525@163.com; [b]xgc@qlu.edu.cn; [c]zjj@qlu.edu.cn; [d]czq@qlu.edu.cn; [e]new-raul@163.com; [f]xch@qlu.edu.cn

Keywords: Self-assembly; Surface modification; self-lubricating; Graphene oxide coating; Si3N4 ceramic

Abstract: Graphene oxide (GO) coated silicon nitride (Si_3N_4@GO) composite powders were prepared with the electrostatic self-assembly mechanism. The experimental results showed that the coating of Si_3N_4 particles by GO can be successfully achieved through the surface modification of Si_3N_4 particles using γ-aminopropyltriethoxysilane (APTES). An advanced Al_2O_3-based ceramic material with the addition of Si_3N_4@GO composite powders (Al_2O_3/(Si_3N_4@rGO)) was fabricated by vacuum hot-pressing sintering (HP) technology, and their mechanical properties and microstructure were analyzed. The microstructure analysis showed that the reduced graphene oxide (rGO) were dispersed homogeneously in the matrix and bonded with the matrix grains tightly. The mechanical properties such as Vickers hardness, fracture toughness and flexural strength was 18.6 GPa, 7.6 MPa $m^{1/2}$ and 626 MPa, respectively. Compared with the Al_2O_3/rGO, the Vickers hardness, fracture toughness and flexural strength were increased by 8.1%, 22.6%, and 28.8%, respectively.

1. Introduction

Structural ceramic composites have received increasing attention over the past few decades owing to their distinctive properties, such as high hardness, high-temperature resistance, high wear resistance, and good chemical stability [1,2]. They have been widely used for many applications, including cutting tools, bearing parts, and valve seats [3]. Enhancing the mechanical properties of ceramic composites was interest for different industrial applications especially in manufacturing industries. Al_2O_3-based ceramic material as one of the widely used material at present, but their poor fracture toughness and flexural strength limit further application and development. In order to decrease its brittleness, many toughening methods are adopted, besides the advanced manufacturing technology. These methods include ZTA (the zirconia transformation toughening), nanometer technology toughening, whisker and fiber toughening, particle dispersion toughening, combined toughening, surface modification toughening, etc. Carbon nanomaterials such as carbon nanotube and grapheme have been attracted as nano-scale fillers in ceramic matrix composites based on their outstanding physical and chemical properties [4, 5]. The carbon nanotube and grapheme reinforced ceramic composites are extensively studied and well documented [6].

Graphene nanoplatelets (GNPs) are two dimensional structure of sp^2 bonded carbon atoms that are arranged in a honeycomb pattern. Its thickness is only 0.3354 nm, which is the thinnest lamellar structure material found at present [7]. In particular, graphene is a monolayer of

carbon atoms arranged in a honeycomb network, exhibit superior electrical conductivity, excellent mechanical flexibility, large surface area, high thermal and chemical stabilities, and so on [8-11]. Because of its excellent properties, GNPs were considered as ideal reinforcing materials for ceramic composites due to their unique mechanical properties and thermal properties. Thus, researchers paid wide attentions to the mechanical, thermal and electrical properties of GNPs reinforced composites with polymer, metal or ceramic as matrix [5,6,12-16]. The additions of GNPs were an effective way to toughen ceramics, which supports findings from previous studies. However, it is factually difficult to obtain a high yield of single layered graphene without subsequent layer agglomeration. GNPs were easy to agglomerate, and a large number of defects and pores were produced after sintering in matrix. So, lead to the decrease of density and mechanical properties of ceramic materials.

Recently it has become evident that composites prepared by spark plasma sintering (SPS) and reinforced with GNPs display anisotropic properties [17].The observed anisotropy was attributed to the preferential orientation of the GNPs along the high conductivity plane, which is perpendicular to the uniaxial pressing direction [18]. Seiner et al. have shown that the presence of 3 wt% of GNPs leads to significant anisotropy of the Young's elastic modulus and the internal friction in Si_3N_4 composites prepared by SPS [19]. However, the self-stratification of GNPs in ceramic matrices is not specific to the SPS technique, but to sintering techniques employing uniaxial pressure. Rutkowskiet al. observed anisotropic mechanical properties in ultrasonic measurements and hardness tests for hot-pressing (HP) (uniaxial pressure) GNPs reinforced Si_3N_4 composites [20]. Furthermore, anisotropic mechanical properties have been observed in calcium phosphate composites with GNPs addition. The mechanical properties (bending strength, fracture toughness, micro-hardness) of the calcium phosphate/GNP composites were greatly improved parallel to the HP direction [21]. For structural ceramics with GNPs addition，the mechanical properties of the composites were greatly improved parallel to the HP direction，but it is poor in vertical direction.

In the present study, the Si_3N_4@GO composite powders were prepared by their Electrostatic Self-assembly Behavior. The composite powders were subsequently mixed with a matrix phase of micron-Al_2O_3, reinforcing phases of Si_3N_4@GO powders to prepare Al_2O_3/(Si_3N_4@rGO) ceramic material by HP sintering. Its microstructure, mechanical properties were examined in detail.

2. Experimental Procedure

Materials and processing. The following starting materials Al_2O_3 (0.2μm), Si_3N_4 (0.2μm), H_2O_2, $C_9H_{23}NO_3Si$, CH_3CH_2OH, $NH_3{\cdot}H_2O$, HCl, MgO (1μm), PEG 6000, Mo (20μm), Ni (20μm), were used for the preparation of Al_2O_3/(Si_3N_4@rGO) ceramic material.

Preparation of Si_3N_4@rGO powders. In order to produce a well-dispersed suspension of Si_3N_4 particles, Si_3N_4 particles were subjected to oxidation using hydrogen peroxide. Si_3N_4 powders were added into the hydrogen peroxide solution at a concentration of 20 % and then stirred and ultrasonically dispersed for 20 min. The obtained suspension was stirred and heated in a thermostatic water bath to a predetermined temperature (80 °C), meanwhile, the time of reaction was 20min. The powder of oxidized Si_3N_4 by H_2O_2 (H_2O_2-Si_3N_4) was prepared under the centrifuge separation and the washing of distilled water. Accordingly, an ultrasonic instrument was utilised to disperse oxidised Si_3N_4 particles into water and alcohol mixture (volume ratio V (water): V (ethanol) =1:1) for 10 min, accompanied by another 1 h sonication in a water bath sonicator. To functionalize surface of Si_3N_4 particles, 4 wt% APTES was added to the prepared suspension. The suspension was subsequently used to adjust pH to the setting value (9) and 3 h of magnetic mixture at the setting temperature (80 °C).

The modified Si_3N_4 powder (APS-Si_3N_4) was obtained after the reaction. The APS–Si_3N_4 suspension was added to the GO suspension (0.5 mg/mL) while stirring at room temperature, GO self-assembly coated APS-Si_3N_4 was prepared due to hydrogen-bonding and then resulted in generation of amide bond between the terminal NH_2 groups on APS–Si_3N_4 particles with COOH groups on GO. The reaction product was centrifuged at 2,000 rpm for 10 min, washed 3 times in absolute ethanol to remove the residue, and then dried at 80 °C for 24 h in a vacuum dryer to obtain the Si_3N_4@GO composite powders.

Preparation of ceramic material. Al_2O_3 and PEG were added to absolute ethanol at the desired mass ratio (Al_2O_3 : PEG was 100 : 2), stirred, and ultrasonically dispersed for 15 min. MgO， Ni and Mo were added to the suspension with the desired volume ratio (MgO : Ni : MO was0.75 : 1.25 : 0.5) and then ultrasonically dispersed for 15 min. The powder slurries were wet-milled with cemented carbide balls (mass ratio m (ball): m (material) =10:1) for 36 h with nitrogen as protective gas. The Si_3N_4@GO powders were added to absolute ethanol at the desired volume ratio and then ultrasonically dispersed for 10 min. The Si_3N_4@GO suspension was added to the slurries and then milled for another period of 4 h. The amount of the added Si_3N_4@GO powders were calculated to make the GO account for 0.75 vol.% in the as-prepared material. After milling, the slurries were dried in vacuum and then sieved using a sifter with a mesh size of 150 μm. The obtained powders were uniaxially compacted into a green body by cold pressing and then HP in vacuum at 1,700 °C for 30 min with a pressure of 30 MPa. Finally, a Al_2O_3/(Si_3N_4@rGO) ceramic disk approximately 42 mm in diameter and 5 mm in thickness was obtained. For comparison, a Al_2O_3/rGO ceramic disk with uncoated GO was also prepared using the same technique.

Material Characterization. The phase composition of the material was identified by X-ray diffraction (XRD, D8-ADVANCE, Bruker AXS Co., Germany). Fourier transform infrared spectrometer (FTIR, FT/IR-470, JASCO, Japan) was used for detection of the information of the chemical bonds of the as-prepared samples. The microstructures were observed using a field-emission scanning electron microscope (SEM, SUPRA^{TM} 55, Carl Zeiss Group, Germany) equipped with an energy-dispersive spectroscope (EDS), transmission electron microscopy (TEM) and highresolution transmission electron microscopy (HRTEM, JEOL-2010, Japan Electronics Co., Ltd., Japan) at an operation voltage of 200 kV. Relative density was determined using the Archimedes method. Flexural strength was tested in a three-point-bending test with a sample size of 3 mm×4 mm×40 mm, using a cross-head speed of 0.5 mm/min on a universal testing machine (WDW-50E). The Vickers hardness was measured on the polished surface using the HV-120 type Vickers hardness tester with a load of 196 N and a loading time of 15 s. Five specimens for each ceramic disk were tested to obtain the respective average values of flexural strength, Vickers hardness and fracture toughness.

3. Results and Discussion

FT-IR spectra. The FT-IR spectra of GO, Si_3N_4, APTES, APS-Si_3N_4 and Si_3N_4@GO are shown in Figure 1. APS-Si_3N_4 have the same band with pure Si_3N_4, As Figure 1 shows, the main characteristic peaks' positions and intensity of APS-Si_3N_4 were expanded, the peak trend of APS-Si_3N_4 is more similar to that of APTES (Figure 1e). The bands at 800～1100 cm^{-1} show skeletal vibration of Si-N. The band at 890 cm^{-1} belonged to the stretching vibration of the Si-N is the typical peak band for Si_3N_4. Busca et al [22] reported there are amine group, silanol, silane and a thin layer of oxygen–rich on the surface of Si_3N_4 nitride particles. The sharp peak around 3750 cm^{-1} presents the stretching vibration of silanol Si-OH. The strong absorption band around 1050-1200cm^{-1} is caused by the stretching vibration of Si-O bond and Si_2N_2O bond on the particle surface. The absorption bands at 3452cm^{-1} and 1400 cm^{-1} belonged to the

stretching vibration peak and bending vibration peak of hydroxylation of -OH on Si_3N_4 surface after water adsorption, respectively.

The bands near 3380cm^{-1} and 1575cm^{-1} are respectively the stretching vibration and bending vibration of $–NH_2$, The stretching vibration peak of $-NH_2$ on modified Si_3N_4 is obviously enhanced, and the peak position is the same as that of APTES (Figure 1b, c). Otherwise, the asymmetric and symmetric stretching vibrations of the C–H bond, located at wavenumbers 2926cm^{-1} and 2854 cm^{-1} on the spectrum of APS-Si_3N_4 is significantly higher than that of Si_3N_4 and the peak position is toward APTES, possibly owing to APTES successfully grafted onto the surface of Si_3N_4 particles, giving a large number of $-CH_2$ functional groups on the surface of the particles. After the silicon powder was nitrided, it was obtained by ball milling with ethanol as medium. In the process of Si_3N_4 particles crushing, the reaction between ethanol and silicon nitride particles formed a stable Si-O-C-R group and the band about C-H appeared in the infrared spectra. For GO, the band at 3452cm^{-1} and 1630cm^{-1} are the stretching vibration and bending vibration of -OH groups formed by GO-adsorbed water molecules, respectively and the band at 1730 cm^{-1} is the vibration of C = O. From Figure 4d, we can see that the infrared spectra of Si_3N_4@GO, which not only includes the infrared peak of GO but also the peak of APS-Si_3N_4 indicates that GO successfully coated on the surface of Si_3N_4 particles.

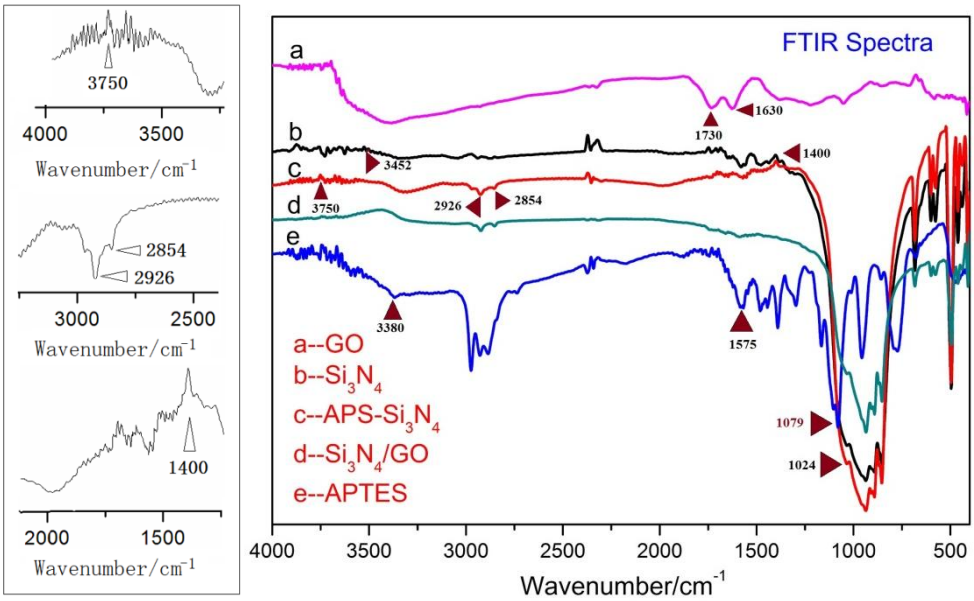

Figure 1. FTIR spectra of powders

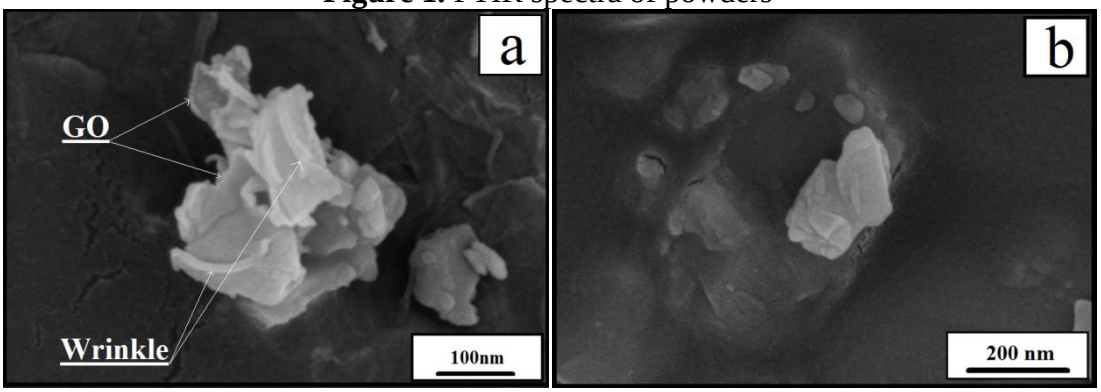

Figure 2. SEM image of (a) Si_3N_4@GO and (b) Si_3N_4 powders

Microstructure analysis of Si_3N_4@GO particles. The microstructure of the Si_3N_4@GO and Si_3N_4 particle surface was examined by SEM, as shown in Figure 2. It can be seen from Figure

2a that wrinkles were observed on the surface of Si_3N_4@GO and the coated particles show a core-shell structure obviously.

The coated structure was further analyzed after the test specimen was ultrasonically treated for 20 min in absolute ethanol. The microstructure of the Si_3N_4 particle surface was examined by TEM before and after coating, as shown in Figure 3a, b. Significant differences were indicated between the Si_3N_4 particles and the Si_3N_4@GO particles. As can be seen from Figure 3b, there is no wrinkle on the surface of the uncoated Si_3N_4 particles, and there is no gauze-like thin layer structure around the particles. As shown in Figure 3a, wrinkles of GO were observed around and on the surface of Si_3N_4 particles. It was shown that the large leaf-like GO nano-sheet appeared, and the low contrast feature indicates the small thickness of the GO. This morphology can reduce the surface energy of GO and keep GO sheets in stable state. The formation of wrinkles can prevent the reunion problem of rGO sheets and maintaining high specific surface area in the ceramics. The formation of wrinkle was caused by the combined effect of the structural feature and surface active group of GO in ultrasonic dispersion process. On the one hand, the two-dimensional structure is difficult to maintain in energy and will be transformed into a stable three-dimensional structure. In addition, the groups on the surface are easily bonded. As illustrated in Figure 3a, b, the results reveal that Si_3N_4 particles are coated perfectly with GO sheets.

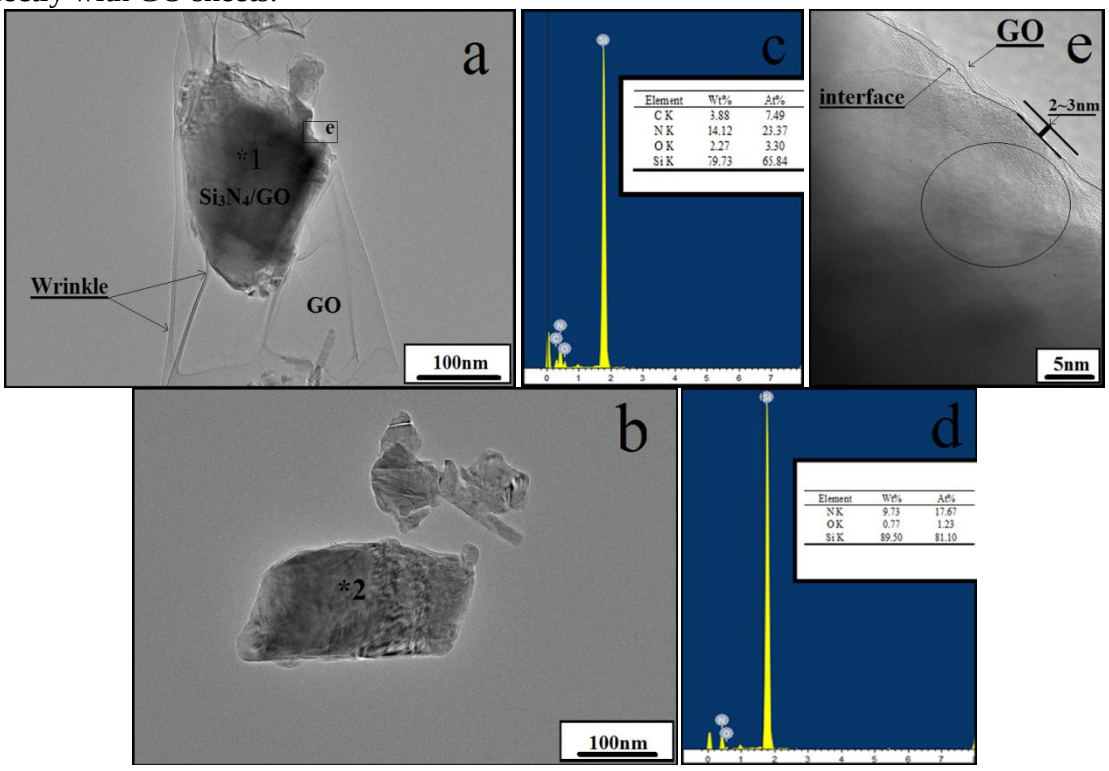

Figure 3. (a), (b) were TEM image of Si_3N_4@GO and Si_3N_4; (c), (d) were EDS spectrum of point 1 and 2; (e) was HRTEM image of Si_3N_4@GO

The morphological characteristics of the nanostructure were further investigated by using HRTEM. Figure 3e is a HRTEM of the Si_3N_4@GO particle in Figure 3a, the "water–striated" structures of GO was observed around in Si_3N_4 particle. The boundary line of Si_3N_4 particles is distinguished by the light transmittance and lattice change of the material. It was observed on the boundary line that Si_3N_4 particles were coated with GO of uniform thickness, and the thickness of the sheet was about 2 to 3 nm. The as-prepared GO is composed of about 3-5 monolayer, as shown in the inset of Figure 3e. The thickness of Si_3N_4 boundary is small, the light transmittance is high, and the apparent GO lattice structure is more obvious. It is found from the area of circle that the lattice structures of Si_3N_4 and GO was overlapped, and with the

increase of Si_3N_4 thickness, the water-like structure of GO on the surface of the particles becomes weak gradually. This indicates that GO was successfully bonded to Si_3N_4 particles.

Figure 3c, d shows the EDS spectra of points 1 and 2 in Figure 3a and b, respectively. Element C was appeared at 1 point, and the weight ratio was 3.88%. In addition, the content of element O at 1 point was significantly higher than that at 2 point, because a large number of oxygen-containing groups were bonded on the surface of Si_3N_4@GO particles. Thus, the surface of point 1 is a GO-coated material, whereas that of point 2 was Si_3N_4.

Mechanical properties and microstructure of materials. The mechanical properties of ceramic composites were measured and the results are summarized in Table 1. The flexural strength, hardness, fracture toughness and relative density of the Al_2O_3/(Si_3N_4@rGO) material are 726MPa, 18.0GPa and 7.6 MPa·$m^{1/2}$, which is increased by about 28.8%, 8.1%, 22.6%, and 1.1%, respectively, relative to those of the Al_2O_3/rGO material.

Table 1. Mechanical properties and relative density of ceramic composites

Sample	Hardness (GPa)	Fracture toughness (MPa·$m^{1/2}$)	Flexural strength (MPa)	Relative density
Al_2O_3/(Si_3N_4@rGO)	18.6±0.36	7.6±0.31	626±14	99.2%±0.12%
Al_2O_3/rGO	17.2±0.26	6.2±0.29	486±13	98.1%±0.13%

4. Conclusions

GO-coated Si_3N_4 powders were prepared by electrostatic self-assemblyin the present study. The strongest electrostatic force was found when the pH value of APS-Si_3N_4 suspension and GO dispersion was 2-4 and 8-10, respectively. The composite powders were subsequently mixed with a matrix phase of Al_2O_3, reinforcing phases of Si_3N_4@Al_2O_3 powders and sintering additives of MgO to prepare Al_2O_3/(Si_3N_4@rGO) ceramic material by HP. The Si_3N_4@rGO particles were dispersed homogeneously in the matrix and the particles were tightly bound therein. The composites was prepared by HP and reinforced with GNPs display isotropic properties. Meanwhile, the problem of regular orientation and agglomeration of rGO in ceramic materials is solved by that addition of coated particles. Its microstructure, mechanical properties, and relative density were superior to those of the Al_2O_3/rGO ceramic material.

Acknowledgements

This work was supported by the National Science Foundation of China (grant no. 51575285).

References

1. Song, N.; Zhang, H.; Liu, H.; Fang, J. Effects of SiC whiskers on the mechanical properties and microstructure of SiC ceramics by reactive sintering. Ceram. Int. 2017, 43, 6786–6790.
2. Demirskyi, D.; Borodianska, H.; Sakka, Y.; Vasylkiv, O. Ultra-high elevated temperature strength of TiB_2-based ceramics consolidated by spark plasma sintering. J. Eur. Ceram. Soc. 2017, 37, 393–397.
3. Deng, J.; Liu, L.; Yang, X.; Liu, J.; Sun, J.; Zhao, J. Self-lubrication of Al_2O_3/TiC/CaF_2 ceramic composites in sliding wear tests and in machining processes. Mater. Des. 2007, 28, 757–764.

4. Sarkar, S.; Das, P.K. Processing and properties of carbon nanotube/alumina nanocomposites: a review. Rev. Adv. Mater. Sci. 2014, 37, 53–82.
5. Mittal, G.; Dhand, V.; Rhee, K.Y.; Park, S.J.; Lee, W.R. A review on carbon nanotubes and graphene as fillers in reinforced polymer nanocomposites. J. Ind. Eng. Chem. 2015, 21, 11–25.
6. Ahmad, I.; Yazdani, B.; Zhu, Y. Recent advances on carbon nanotubes and graphene reinforced ceramics nanocomposites. Nanomaterials, 2015, 5, 90–114.
7. Novoselov, K.S.; Geim, A.K.; Morozov, S.V.; Jiang, D.; Zhang, Y. Electric field effect in atomically thin carbon films. Science, 2004, 306, 666-669.
8. Balandin, A.A.; Ghosh, S.; Bao, W.; Calizo, I.; Teweldebrhan, D.; Miao, F. Superior thermal conductivity of single-Layer graphene. Nano. Lett. 2008, 8, 902-907.
9. Bolotin, K.I.; Sikes, K.J.; Jiang, Z.; Lima, M. K.; Fudenberg, G. Ultrahigh electron mobility in suspended graphene. Solid State Commun. 2008, 146, 351-355.
10. Stoller, M.D.; Park, S.; Zhu, Y.; An, J.; Ruoff, R.S. Graphene-based ultracapacitors. Nano Lett, 2008, 8, 3498-3502.
11. Lee, C.; Wei, X.; Kysar, J.W.; Hone, J.; Measurement of the elastic properties and Intrinsic strength of monolayer graphene. Science, 2008, 321, 385-388.
12. Dusza, J.; Morgiel, J.; Duszová, A.; Kvetková, L.; Nosko, M. Microstructure and fracture toughness of Si_3N_4 + graphene platelet composites. J. Eur. Ceram. Soc. 2012, 32, 3389-3397.
13. Dutkiewicz, J.; Ozga, P.; Maziarz, W.; Pstruś, J.; Kania, B. Microstructure and properties of bulk copper matrix composites strengthened with various kinds of graphene nanoplatelets. Mater. Sci. Eng. A, 2015, 628, 124-134.
14. Bisht, A.; Srivastava, M.; Kumar, R.M.; Lahiri, I.; Lahiri, D. Strengthening mechanism in graphene nanoplatelets reinforced aluminum composite fabricated through spark plasma sintering. Mater. Sci. Eng. A, 2017, 695, 20-28.
15. Bafana, A.P.; Yan, X.; Wei, X.; Patel, M.; Guo, Z. Polypropylene nanocomposites reinforced with low weight percent graphene nanoplatelets. Compos. Part B-eng., 2017, 109, 101-107.
16. Seretis, G.V.; Kouzilos, G.; Manolakos, D.E.; Provatidis, C.G. On the graphene nanoplatelets reinforcement of hand lay-up glass fabric/epoxy laminated composites. Compos. Part B-eng., 2017, 118, 26-32.
17. Tapasztó, O.; Tapasztó, L.; Lemmel, H.; Puchy, V.; Dusza J. High orientation degree of graphene nanoplatelets in silicon nitride composites prepared by spark plasma sintering. Ceram. Int., 2016, 42, 1002-1006.
18. Ramirez, C.; Garzón, L.; Miranzo, P.; Osendi, M.I.; Ocal, C. Electrical conductivity maps in graphene nanoplatelet/silicon nitride composites using conducting scanning force microscopy. Carbon, 2011, 49, 3873-3880.
19. Seiner, H.; Sedlák, P.; Koller, M.; Landa, M.; Ramírez, C.; Osendi, M.I.; Belmonte, M. Anisotropic elastic moduli and internal friction of graphene nanoplatelets/silicon nitride composites. Compos. Sci. Technol, 2013, 75, 93–97.
20. Rutkowski, P.; Stobierski, L.; Zientara, D.; Jaworska, L.; Klimczyk, P.; Urbanik, M. The influence of the graphene additive on mechanical properties and wear of hot-pressed Si_3N_4 matrix composites. J. Eur. Ceram. Soc., 2015, 35, 87–94.
21. Zhao, Y.; Sun, K.N.; Wang, W.L.; Wang, Y.X.; Sun, X.L.; Liang, Y.J.; Sun, X.N.; Chui P.F. Microstructure and anisotropic mechanical properties of graphene nanoplatelet toughened biphasic calcium phosphate composite. Ceram. Int. 2013, 39, 7627–7634.
22. Ramis, G.; Busca, G.; Lorenzelli, V.; Baraton, M.I.; Merle-Mejean, T. FT-IR Characterization of High Surface Area Silicon Nitride and Carbide. Springer Netherlands, 1989, 173, 173-184.